tures. A 45-degree straight line drawn through the origin connects all these calibration points; this suggests absence of radio-frequency saturation, good field uniformity, and a constant line-shape function, all factors that tend to make peak area directly proportional to the number of resonating protons per unit volume of sample (*2, 3*).

The variation in the liquid-water content of cod fillet with temperature is shown in Fig. 3; the data, for the same sample of tissue, indicate that rapid decrease in content between 0° and −10°C is followed by a slow decrease at lower temperatures. Quantitative measurements were made down to −20°C. Qualitative measurements on a wide-band spectrometer, at temperatures below −20°C, show that the liquid-water spectrum exists at −68°C and disappears at about −70°C (*4, 5*).

Figure 4 shows the variation in absorption-peak width with temperature. Peak width, measured at 0.6 of peak maximum, increases with decreasing temperature, suggesting a loss of mobility, or increase in structuring of water molecules, with decrease in extent of the liquid phase and in temperature. Water-peak widening has been reported (*6*) for water in clays at temperatures below 0°C, as well as an increase in water-peak width as the water content of various natural materials, particularly starch, decreases (*7*).

Peak width at temperatures between 20° and 0°C is about 10 cy/sec, compared with about 2 cy/sec for pure distilled water and 7 cy/sec for the "Homo-adjust" standard (a solution of paramagnetic salts) used with the A-60 machine. Below 0°C the peak widens rapidly, reaching 140 cy/sec at −19°C. Broadening of NMR water signals (or decrease in transverse relaxation time) in the presence of DNA, human cells, starches, and other materials (*8, 9*) has been ascribed to loss of mobility and structuring of the liquid water by processes such as H-bonding, adsorption, gelation, hydration, and others. The broadened tissue peak is still much narrower than a pure-ice peak; comparison of the two on a wide-band spectrometer (*5*) showed the peak width of pure ice to be 70 times greater than that of the liquid water of fish muscle at −16°C.

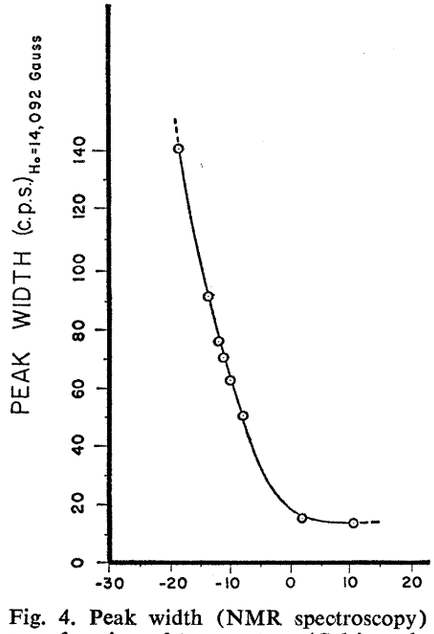

Fig. 4. Peak width (NMR spectroscopy) as a function of temperature (Celsius, abscissa).

The rapid freezing rate followed by the slow freezing (Fig. 3) may be interpretable in terms of freezing of "free" and "bound" water phases, the concept of "bound" water having something of a tradition in discussions of cellular water (*9, 10*). Figure 4, however, showing no sharp slope changes below 0°C, indicative of a disappearance of phase, suggests that the change in binding is gradual and probably involves a spectrum of binding energies.

Most estimates of the extent of liquid phase in frozen tissue, based on calorimetric, histological, dilatometric, and thermal-conductivity observations, agree that most of the liquid phase is solidified at or above −20°C. Estimates of the temperature of complete solidification of animal tissue vary from −20°C to −65°C (*10*). Riedel (*11*) reports that cod muscle freezes completely below −65°C.

M. V. Sussman
L. Chin
Department of Chemical Engineering, Tufts University, Medford, Massachusetts

References and Notes

1. With a Varian A-60 high-resolution spectrometer fitted with a model V-6057 controlled-temperature probe, which was adjusted for optimum field homogeneity and "ringing" before each run.
2. T. M. Shaw and R. H. Elsken, *J. Appl. Phys.* **26**, 313 (1955); *Anal. Chem.* **27**, 1983 (1955).
3. J. A. Pople, W. G. Schneider, H. J. Bernstein, *High Resolution NMR Spectroscopy* (McGraw-Hill, New York, 1959).
4. The water content of muscle of fresh cod at probe temperature (38°C), determined by NMR measurement on 51 samples taken from five fish, is 81 ± 2 percent. Precision of an individual peak-area measurement is estimated to be within 1.5 percent.
5. Wide-line spectra were run for us by Rainer Mattes in E. Rochow's laboratory at Harvard University; we thank both.
6. T. H. J. Wu, *Geophys. Res.* **69**, 1083 (1964).
7. T. M. Shaw and R. H. Elsken, *J. Chem. Phys.* **21**, 565 (1953).
8. B. Jacobsohn, W. A. Anderson, J. T. Arnold, *Nature* **173**, 772 (1954); O. Hechter, T. Wittstruck, N. McNiven, G. Lester, *Proc. Nat. Acad. Sci. U.S.* **46**, 783 (1960); E. Odelblad, *Ann. N.Y. Acad. Sci.* **83**, 189 (1959).
9. C. B. Bratton, A. L. Hopkins, J. W. Weinberg, *Science* **147**, 738 (1965).
10. R. M. Love, in *Cryobiology*, H. T. Meryman, Ed. (in press), chap. 7.
11. L. Riedel, *Kaltetechnik* **8**, 374 (1956).
12. This work was supported by the U.S. Bureau of Commercial Fisheries Technological Laboratory, Gloucester, Mass.

12 November 1965

Manganese Nodules: Their Evolution

Abstract. *That manganese nodules and adjacent deep-sea sediments are accumulating manganese at almost the same rate has been established by thorium-230 dating of both sediments and nodules of known manganese content. The rate of manganese deposition is nearly constant over the world oceans. A relatively simple model of nodule evolution explains the distribution of manganese nodules between sediment column and sediment-water interface; the model appears to apply to other trace elements such as copper, nickel, and cobalt.*

Since Murray and Renard (*1*) first reported the discovery of manganese nodules by the *Challenger* expedition (1873–76), many workers have speculated regarding the origin of these ferromanganese oxide concretions. Kuenen (*2*) reviewed the evidence that the nodules grow by slow accumulation of authigenic manganese. More recently Bonatti and Nayudu (*3*) discussed indications that manganese nodules are formed by rapid accumulation of manganese coming from submarine volcanic exhalates. The composition, mineralogy, occurrence, and theories regarding the evolution of nodules were recently discussed extensively by Mero (*4*) and Menard (*5*).

We propose the following simple model, based on our findings, for the evolution of manganese nodules. The relatively constant rates at which manganese accumulates in deep-sea sediments (Table 1) indicate that there is a rather uniform "rain" of manganese over the entire ocean floor. Whereas most of this manganese is incorporated into deep-sea sediments, hard bodies such as sharks' teeth and volcanic fragments lying on the sediment surface

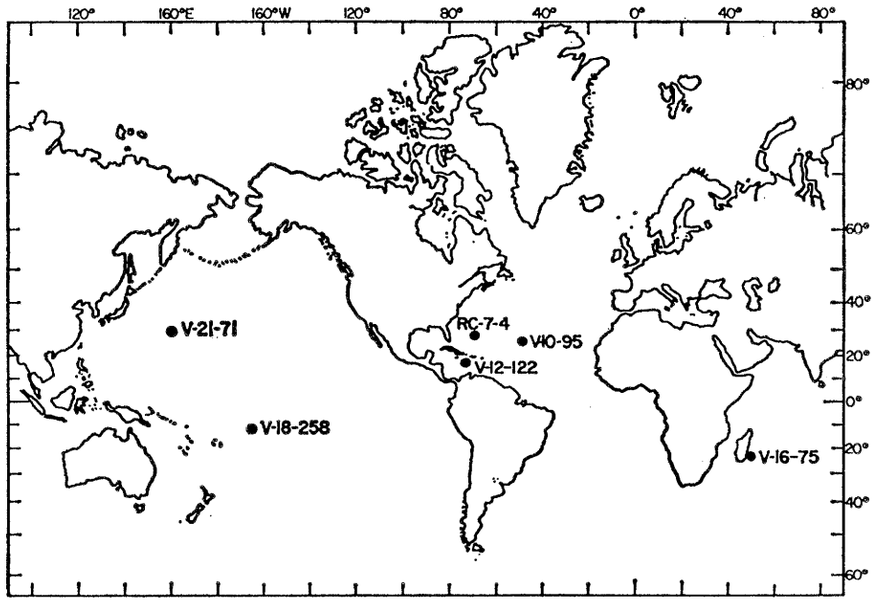

Fig. 1. Sources of samples.

accumulate manganese according to their geometric cross sections. Because of some unknown mechanism these hard bodies are continually rolled over the ocean floor and kept free of the depositing sediments; this process, with the hard bodies accumulating manganese, continues until the bodies reach a certain critical size beyond which they are too heavy to be moved; they are then covered by the sediment and preserved therein. This hypothesis makes several predictions which are subject to experimental verification:

1) The rate of growth of the radius of a nodule is given by

$$dr/dt = S/4\rho f$$

where S is the sedimentation rate of manganese oxide, ρ is the nodule density, and f is the fraction of manganese oxide in the nodule.

2) The ratio (R) of the probability of a nodule occurring in the top of a core to that of one occurring within a unit length of a core is

$$R = 4\rho f r^*/C$$

where r^* is the average radius of a nodule upon burial (on reaching a certain critical size) and C is the weight percentage of manganese oxide in the sediment.

3) Other trace metals, having chemical properties similar to those of manganese and showing unusually high concentrations in ocean sediments, should be distributed between nodule and sediment, as is manganese; examples are cobalt, nickel, and copper.

We have compared our predictions with natural processes by making measurements and by reference to the literature. We determined the sedimentation rates of manganese (Table 1) by measuring its concentrations in six cores (Fig. 1) dated by the Th^{230} and Pa^{231} methods. Total-sediment-accumulation rates for five of these cores have been reported (*6*). The rate for core V-21-71, 0.25 cm 10^{-3} yr^{-1}, is of particular interest since a nodule was present in the top of the core. Sediment is thus accumulating at normal rates in areas in which manganese nodules are formed.

Manganese contents were determined by neutron-activation analysis; the 0.85-Mev γ peak of the 2.58-hour-half-life Mn^{56}, produced by the Mn^{55} (n, γ) Mn^{56} reaction, was measured. The technique was similar to Stueber's (*7*) except that powdered MnO_2 was used as the standard. Decay curves for about 20 samples proved satisfactory. The ratio of the 0.85-Mev γ peak to the 1.81-Mev γ peak of Mn^{56}, computed for many of the spectra, was equal for sample and standard. Triplicate analyses of the geochemical standard W-1 gave the value of 0.15 percent MnO; the favored value (*8*) is 0.16 percent MnO. The absolute error for all analyses (Fig. 2) is less than 10 percent.

We measured the growth rates of two manganese nodules dredged at station V-21-71. Successive portions from their surfaces, corresponding to thicknesses of about 0.2 mm, were scraped from 1-cm^2 areas; the powder obtained was counted for gross alpha activity with a scintillation counter. The logarithm of the gross alpha activity decreased linearly with depth, and the growth rate was computed from these curves, on the assumption that all activity was due to Th^{230} and its daughters in equilibrium; two direct Th^{230} measurements by alpha-spectrometry gave results compatible with this interpretation. Growth rates (Fig. 3) are estimated at about 3 mm 10^{-6} yr^{-1}.

We can now evaluate our model's predictions. We must emphasize that,

Table 1. Manganese accumulation rates, from cores. Bulk density of cores taken to be 1.0 g cm^{-3}; that of Mn nodule, 2.8 cm^{-3}. Cal., calcareous.

Core			MnO		
Number and source	Depth (m), type	Deposition rate (mm 10^{-3} yr^{-1})	Av. content, last $x \times 10^5$ yr (wt %)	Sedimentation rate (mg cm^{-2} 10^{-3} yr^{-1})	
				Total	Authigenic*
RC7-4, 29°14′N, 74°15′W	4667, cal. silty clay†	26	0.18	4.7	2.5
V12-122, 17°00′N, 74°24′W	2800, cal. ooze†	28	0.15	4.2	3.1
V10-95, 26°31′N, 51°47′W	5190, red clay	3.7	0.73	2.7	2.3
V16-75, 22°13′S, 50°23′E	4630, red clay	5.8	0.49	2.7	2.2
V21-71, 27°54′N, 162°31′E	5860, red clay	2.5	0.58	1.5	1.3
V21-71, 27°54′N, 162°31′E	5860, Mn nodule	3×10^{-3}	35‡	1.2	1.2
V18-258, 11°52′S, 165°45′W	5528, red clay	1.7	1.6	2.7	2.5

* Assuming that detrital silicate fraction of sediment contains 0.104 percent MnO (the observed content of shales). † Average $CaCO_3$ content: 20 percent in RC7-4, 64 percent in V12-122. ‡ Estimated.

Table 2. Relation between authigenic Mn, Co, Ni, and Cu in nodules and in adjacent sediment. Data on concentration in clays and shales are from Turekian and Wedepohl (*13*); on Mn nodules, from Mero (*4*).

Element	In red clay: excess/ excess Mn	In nodules: concentration/ Mn concentration
Co	0.009	0.014
Ni	.03	.04
Cu	.04	.02

because of certain arbitrary factors concerning choice of values for certain parameters, the following comparisons are considered meaningful only within one order of magnitude.

1) The predicted rate of growth for nodules from station V-21-71 is easily calculated. On the assumption that S is 0.0013 g cm^{-2} per 10^3 years, F is 0.35, and ρ is 2.5 g cm^{-3}, the model predicts a value for dr/dt of about 4 mm 10^{-6} yr^{-1}, in excellent agreement with the measured value of 3 mm 10^{-6} yr^{-1}. These rates are also consistent with the previously reported value of < 10 mm 10^{-6} yr^{-1} for a nodule dredged from the North Pacific (*9*).

2) If the average MnO concentration (C) in deep-sea sediments is assumed to be 0.6 percent, and if f is 0.30, ρ is 2.5 g cm^{-3}, and r* is 1.5 cm, according to the model, the ratio of the number of nodules observed in a core top to the number in each meter of core length should be about 7. Comparison is provided by Menard's reported value of 2, derived from a survey of 34 nodule-bearing cores 1 m long (*5*, *10*). Our observations on 48 cores having nodules at less than 1 m of depth, from the Lamont collection, yield a value of 1.7. [Of the 54 Lamont cores (*11*) 28 had nodules only in the top, 6 had them both in the top and within the first meter, and 14 had them only within the first meter.] When one considers that these results are for areas well removed from the sites of our radiochemical observations, the agreement is satisfactory.

3) The model predicts that elements that are highly concentrated in red clays, and that are similar in chemical properties to manganese, should be concentrated to the same degree in nodules. The excesses of Co, Ni, and Cu relative to the excess of Mn in red clays (excess is defined as concentration in red clay minus concentration in shale) are compared with the concentrations of these elements relative to that of Mn in nodules (Table 2). Despite the complications caused by large uncertainties in these values, excesses of these elements in clays and their concentrations in nodules relative to Mn are similar.

Agreement between prediction and observation implies that the model is basically valid. The major implication of this conclusion is that the occurrence of manganese nodules does not need very peculiar environmental conditions; it is to be expected if one assumes that the nuclei can accumulate authigenic matter as easily as the mud at the surface of the adjacent sediments. A major mystery still unsolved is the mechanism by which these nodules continually move over the surface of the sediment.

Goldberg and Arrhenius (*12*) have reported that the residence time of manganese in the ocean is about 7000 years, a value much greater than the mixing time of the oceans (*13*). Because manganese in deep-sea sediments is principally authigenic, one may infer that manganous ion is rather homogeneously distributed throughout the oceans and that the sedimentation rate of manganese in the different oceans is quite constant. We have calculated sedimentation rates (S) of authigenic manganese by assuming that detrital manganese accounts for 0.104 percent [the MnO content of shale (*14*)] of

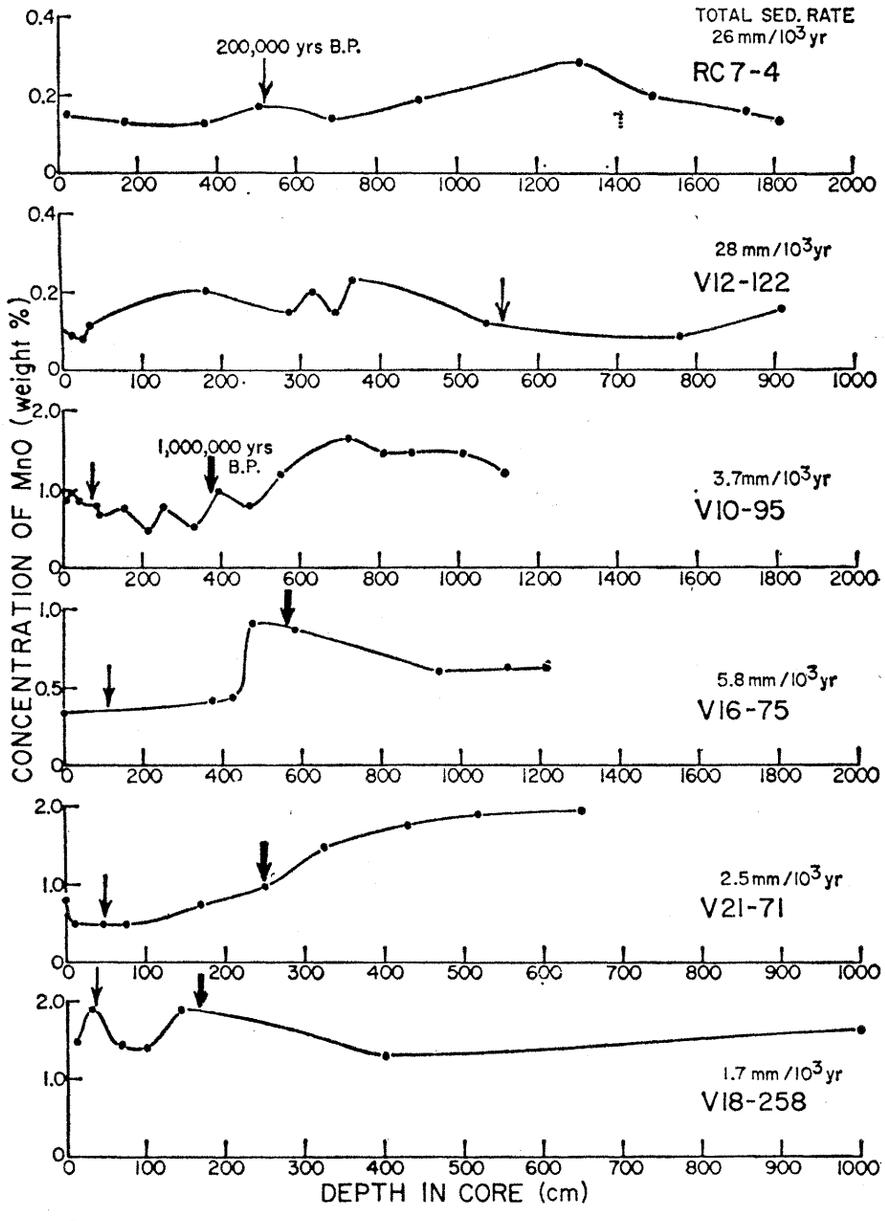

Fig. 2. Concentration of MnO as a function of depth in six deep-sea cores.

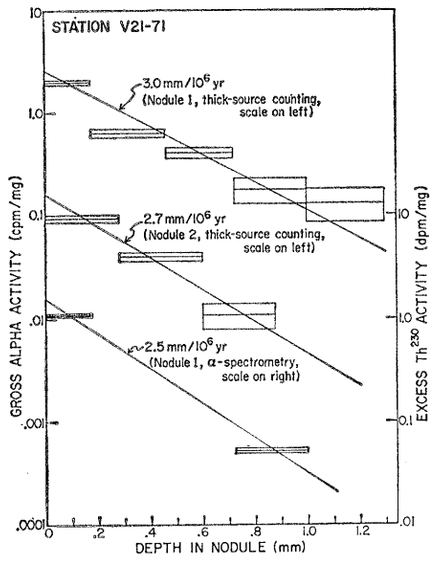

Fig. 3. Accumulation rate for Mn nodules from station V-21-71, northwestern Pacific.

the clay fraction and by substracting this from the total manganese content (Table 1). The striking feature of these results is that, as expected on the basis of the above arguments, sedimentation rates for authigenic manganese are remarkably constant. This finding is true for very different types of sediment in which manganese content and accumulation rates differ by an order of magnitude.

The manganese profiles for V-21-71, V-16-75, and V-10-95 are noteworthy. Concentration of manganese oxide in each of these cores increases substantially at a depth corresponding to an extrapolated age of about 10^6 years; if this increase reflects primary differences in the manganese : sediment ratio of accumulation, then either total sedimentation has been faster during the last 10^6 years or the manganese deposition rate has been much lower during this period. These possibilities may be resolved by other dating methods (such as by Be^{10}) that promise to extend the chronology of sedimentation. If, in addition to areal constancy, the sedimentation rate of manganese has been constant through time, measurement of manganese concentrations in sediments will provide a useful tool for analyzing sedimentation rates.

MICHAEL L. BENDER
TEH-LUNG KU
WALLACE S. BROECKER
Lamont Geological Observatory,
Columbia University,
Palisades, New York

References and Notes

1. J. Murray and A. Renard, Challenger *Reports* (1891), 525 pp.
2. P. H. Kuenen, *Marine Geology* (Wiley, New York, 1950), 551 pp.
3. E. Bonatti and Y. R. Nayudu, *Amer. J. Sci.* **263**, 17 (1965).
4. J. L. Mero, *The Mineral Resources of the Sea* (Elsevier, New York, 1964), 312 pp.
5. H. W. Menard, *Marine Geology of the Pacific* (McGraw-Hill, New York, 1964), 271 pp.
6. W. M. Sackett, in *Symposium on Marine Geochemistry*, Graduate School Oceanog., Rhode Island Univ., Ed. (1965); T. L. Ku, *J. Geophys. Res.* **70**, 3457 (1965); ——— and W. S. Broecker, *Science*, in press.
7. A. M. Stueber, thesis, Univ. of California, San Diego (1965).
8. M. Fleischer and R. E. Stevens, *Geochim. Cosmochim. Acta* **26**, 525 (1962).
9. E. D. Goldberg, in *Oceanography*, M. Sears, Ed. (AAAS, Washington, D.C., 1961), p. 583.
10. Cores from Scripps Institution of Oceanography.
11. Taken during five cruises (V16–V20) of R.V. *Vema* and totaling more than 1000 cores.
12. E. D. Goldberg and G. O. S. Arrhenius, *Geochim. Cosmochim. Acta* **13**, 58 (1958).
13. W. S. Broecker, in *The Sea* (1963), vol. 2, p. 88.
14. K. K. Turekian and K. H. Wedephol, *Bull. Geol. Soc. Amer.* **72**, 175 (1961).
15. Neutron-activation analyses were by courtesy of Industrial Reactor Laboratories, Plainsboro, N.J. Arthur de St. Maurice and Owen Hingher assisted with the experiments. W. Cassidy and P. Gast gave helpful advice regarding activation analysis. Paul Smith helped with $CaCO_3$ analyses on core RC-7-4 and with the survey of nodules in Lamont cores. Marylou Zickl typed the manuscript and John Brokaw did the drafting. Supported by NSF (predoctoral fellowship for M.L.B.) and by AEC contract AT(30-1)3139. Lamont Geological Observatory contribution No. 867.

1 November 1965

Gene-Specific Messenger RNA: Isolation by the Deletion Method

Abstract. *Messenger RNA molecules, homologous to a small portion of the genome of bacteriophage T4, have been isolated. RNA fragments specific to the rII A and the rII B cistrons have been separated by hybridization with DNA isolated from appropriate deletion mutants. An RNA species homologous in nucleotide sequence to a defined part of the rII A cistron has been identified.*

The separation of a gene-specific messenger RNA (mRNA) species from a multitude of structurally similar, but informationally different, messengers can be accomplished in principle by either of two procedures. In some instances, a limited number of genes can become integrated into the genome of a transducing phage, and as such be separated from the bacterial genome; this DNA can be made to form complexes selectively with its homologous RNA (*1*). In those cases, where an episomal element is not available for the selection of a particular segment of DNA, a deletion mutant lacking the gene to be studied can be used to remove, by hybridization, all but the desired mRNA species.

The method of complex formation between mRNA and episomal DNA is straightforward once the selection of the proper DNA piece has been achieved. This selection is, however, so far limited to only three experimental systems (*1*). Since there are many more genes known for which deletion mutants are available, the method of removal by hybridization would provide a wider range of application. The experimental difficulty encountered here is that the first step of hybridization, namely, elimination of all undesired mRNA species, has to be quantitative.

A previous attempt (*2*) has revealed the feasibility of purifying RNA, specific for the rII region of bacteriophage T4, by this approach. In this report we describe a general procedure for the isolation and the detection of gene-specific mRNA. The procedure applies the observations that nitrocellulose binds single-stranded DNA (*3*) and that the bound DNA is still capable of forming complexes with homologous RNA (*4*).

DNA was extracted by shaking concentrated bacteriophage stocks three times with phenol saturated with 0.01*M* tris (*p*H 7.2) and then by precipitating the DNA from the aqueous layer with two volumes of ethanol. The DNA was collected on a glass rod and stored as dried fibers. Before use a portion of the DNA was dissolved in low-salt buffer (*5*) and denatured by heat at a concentration of 0.3 mg/ml; the denatured DNA was cooled rapidly, adjusted to high-salt buffer, and pipetted into a suspension of nitrocellulose powder in high-salt buffer; this mixture was then rapidly stirred for 5 minutes. The suspension of nitrocellulose (type RS, Hercules Powder Co.) was prepared by grinding it in high-salt buffer in a mortar, passing the slurry through a 40-mesh stainless-steel sieve, decanting to remove fine particles, and washing with high-salt buffer for 2 hours at room temperature. A slurry of 10 mg of DNA of bacteriophage T4r+ (wild type) on nitrocellulose was poured into a jacket column of 15 mm diameter to yield a column height of 12 cm. A small amount of plain nitrocellulose was packed on top of it, and on this layer was placed a 12-cm column of nitrocellulose containing 10 mg of DNA of the mutant phage r1272 [a